Phonon dispersion relations of zinc oxide: Inelastic neutron scattering and *ab initio* calculations

J. Serrano,[1,*] F. J. Manjón,[2] A. H. Romero,[3] A. Ivanov,[4] M. Cardona,[5] R. Lauck,[5] A. Bosak,[6] and M. Krisch[6]
[1]*ICREA-Departament de Física Aplicada, EPSC, Universitat Politècnica de Catalunya, Carrer Esteve Terradas 15, E-08860 Castelldefels, Spain*
[2]*Instituto de Diseño para la Fabricación y Producción Automatizada, MALTA Consolider Team, Universitat Politècnica de València, Cno. de Vera s/n, 46022 València, Spain*
[3]*CINVESTAV, Departamento de Materiales, Unidad Querétaro, 76230 Querétaro, Mexico*
[4]*Institut Laue Langevin, 156X, 38042 Grenoble cedex 9, France*
[5]*Max Planck Institut für Festkörperforschung, Heisenbergstraße 1, D-70569 Stuttgart, Germany*
[6]*European Synchrotron Radiation Facility, BP 220, 38043 Grenoble cedex 9, France*
(Received 17 February 2010; revised manuscript received 27 April 2010; published 24 May 2010)

Zinc oxide is a key material for optoelectronic applications, whose transport properties are typically dominated by the lattice vibrations. We report here the phonon-dispersion relations of wurtzite ZnO at 10 K, as determined by using inelastic neutron scattering. The experimental data are analyzed with the aid of *ab initio* calculations based on density-functional perturbation theory. A complete picture of the lattice dynamics is drawn from the present results, thus contributing to the understanding of mechanical, thermodynamical, and transport properties of wurtzite optoelectronic materials.

DOI: 10.1103/PhysRevB.81.174304 PACS number(s): 61.05.fg, 63.20.dk, 78.55.Et

I. INTRODUCTION

ZnO in powder form is largely utilized in pigments, sun blocker lotions, adhesives and ceramics. More recently, it has fostered new applications in the optoelectronic industry due to the direct band gap of 3.4 eV. Applications in the ultraviolet energy range have been further developed after nanowires of ZnO became available,[1,2] including blue light-emitting diodes,[3] field-effect transistors,[4] nanosensors,[2] UV nanolasers,[5] and in high-efficiency solar cells,[6,7] and UV photodetectors.[8] The large attraction for this material has prompted several reviews in recent years.[9–12]

Thermodynamical properties, such as heat transport and specific heat, play an important role in the understanding of the limits of ZnO for optoelectronic applications. These properties are mediated by the quantum vibrations of the atomic lattice, as described by the phonon-dispersion relations. Mechanical properties, such as the elastic stiffness constants, can also be extracted from the lattice dynamics. Despite the thorough understanding of the optical and electronic properties of ZnO, there is a lack of experimental information on the phonon-dispersion relations throughout the whole Brillouin zone (BZ), which can be mainly accessed by two techniques: inelastic neutron scattering (INS) and inelastic x-ray scattering (IXS).[13] Contrary to other semiconductors used in optoelectronics, such as GaN and AlN,[14,15] no IXS experiments have been reported for ZnO. The scarce information available for ZnO stems from INS experiments performed in the 1970s (Refs. 16–18) that reveal some of the acoustic branches along selected high-symmetry directions. These INS results, complemented by Raman data,[19–22] gave rise to unreliable semiempirical models of the phonon-dispersion relations.[18] In order to obtain a more accurate description of the lattice dynamics, one can choose between two complementary strategies: a first-principles calculation and an IXS/INS experiment. We reported in Ref. 23 an extensive investigation of the lattice dynamics of wurtzite ZnO using *ab initio* calculations.

In this paper we report INS experiments on a single crystal of wurtzite ZnO, performed at the Institut Laue Langevin in Grenoble, France. The INS data, partially reported in a conference proceedings,[24] are compared with *ab initio* calculations. Besides this comparison, we include here a table with the experimental frequencies obtained at high-symmetry points, which may be of use to design reliable semiempirical models for the calculation of lattice dynamical properties such as heat transport and thermal conductivity, for both bulk ZnO and related nanostructures.

II. EXPERIMENTAL METHOD

Inelastic neutron-scattering experiments were conducted on a single crystal of ZnO of 30×15 mm^2 size in length and diameter, respectively, with the length along the c axis. The experiments took place at the hot source IN1 triple axis spectrometer of the Institut Laue Langevin in Grenoble, France. The sample was mounted with the c-axis vertical, i.e., perpendicular to the spectrometer scattering plane. An Orange He closed-cycle cryostat was employed in order to avoid temperature-renormalization effects on the phonon frequencies and multiple scattering, and thus to better compare with the results of *ab initio* calculations. INS spectra were obtained at 10 K with an energy resolution of 4 meV, full width at half maximum, at the elastic configuration, as defined by Soller-slit collimators placed along both the incoming and scattered beams. The INS scans were performed in the so-called constant final-momentum mode, k_f, with $k_f=65$ nm^{-1}.

III. *AB INITIO* CALCULATIONS

We performed *ab initio* calculations of the lattice dynamics of wurtzite ZnO within the frame of density-functional

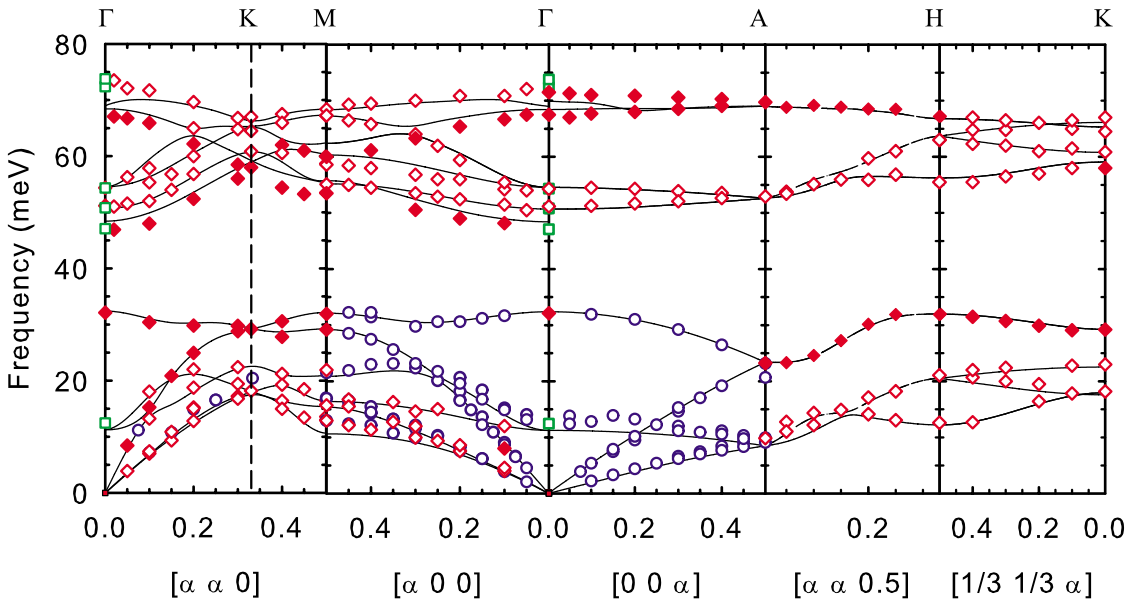

FIG. 1. (Color online) Phonon-dispersion relations of ZnO along the main symmetry directions. Solid and open diamonds (red) represent INS data of this work obtained with a scattering geometry that selects modes polarized along the c axis and in-plane, respectively. Open circles (blue) correspond to INS data reported in Refs. 17 and 18, and squares (green) display available Raman data at 7 K in Ref. 29. The solid curves display the results of *ab initio* calculations reported in Ref. 23. The x-axes are given in reciprocal lattice units.

perturbation theory, as implemented in the ABINIT package.[25–28] The quality of these lattice dynamical calculations was already tested by comparing them with experimental data for the pressure dependence of Raman frequencies and linewidths,[29,30] and also with the measured dependence of the specific heat on isotopic mass.[31] The original calculations, reported in Ref. 23, were extended in this work by using a grid of $10\times10\times8$ points in the irreducible Brillouin zone in order to improve convergence of the phonon frequencies. Additionally, here we employed pseudopotentials generated using the Troullier-Martins scheme[32] for both, the local density approximation[33] and the generalized gradient approximation[34] for the exchange and correlation energy. No significant differences were observed with respect to the phonon-dispersion relations reported in Ref. 23, where more details about the calculations can be found.

IV. RESULTS AND DISCUSSION

Figure 1 compares our INS data (diamonds, red) for the modes along the main symmetry directions of the BZ with those previously reported in the literature (circles, blue)[17,18] and Raman data (squares, green) at 7 K.[29] The x-axes are given in reciprocal lattice units (r.l.u.). Although emphasizing more the optical branches, our INS data are in good agreement with those reported previously for the acoustic branches.[17,18] Note that our INS data were obtained at 10 K whereas those of Refs. 17 and 18 were acquired at room temperature. The effect of temperature on the phonon frequencies is completely masked by the energy resolution. The solid symbols represent data obtained using a scattering geometry with a reciprocal vector along the hexagonal axis whereas open symbols correspond to data obtained using an in-plane polarization. Our INS data are in excellent agreement with the calculated results, displayed by solid curves.

Table I shows the phonon frequencies at the Γ point of the BZ as determined by INS and *ab initio* calculations, compared to available Raman data measured at 7 K.[29] The *ab initio* frequencies were obtained by linear response calculations at the Γ point, therefore they are slightly different from those obtained using interpolation schemes on a grid of dynamical matrices. Calculated frequencies underestimate the Raman data by up to 7%, for the longitudinal optic modes. This is close to the accuracy expected for the calculations, given the fact that we used the theoretically relaxed unit-cell volume and we neglected self-energy corrections[35] in the calculation of the band structure. Furthermore, the calculations reveal a reverse ordering of the A_1 and E_1 longitudinal optic modes, as displayed both in Table I and in Fig. 1, probably due to deficiencies in the evaluation of the electrostatic contribution to the splitting between transverse and longitudinal optical modes. These deficiencies are usually ascribed to an

TABLE I. INS phonon frequencies of ZnO at the Brillouin-zone center measured at 10 K, compared to Raman data measured at 7 K and *ab initio* calculations, in meV.

Symmetry	INS	*Ab initio*	Raman
E_2	12.2	11.3	12.4
B_1	32.1	32.4	Silent
A_1	46.9	48.4	47.1
E_1	51.1	50.7	50.8
E_2	54.4	54.6	54.3
B_1	68.4	68.4	Silent
E_1	73.5	69.0	73.8
A_1	71.1	70.0	72.4

incorrect calculation of the infinite frequency dielectric constant, which might be corrected by employing a more accurate electronic band structure, e.g., by using self-energy corrections.[36,37] It is worth noticing the excellent agreement between INS and calculated data sets for q points along the boundaries of the BZ, which are not influenced by the calculation of the dielectric constants.

We report also in Table I the modes of B_1 symmetry at the Γ point, at 259 and 556 cm^{-1}, which are not accessible with either Raman or infrared spectroscopy due to symmetry-related selection rules. These modes may become activated by disorder effects in alloys, by doping with other atoms, or by inducing defects. Besides the excellent agreement with the calculated wave numbers, 261 and 556 cm^{-1}, the INS data agree well with modes observed at 276 and 580 cm^{-1} in Ga- and N-implanted ZnO.[38] The assignment of these modes to disorder-activated Raman signatures was made in an earlier work[39] guided by *ab initio* calculations and it is further confirmed by these INS results.

Table II summarizes calculated and experimentally obtained phonon frequencies corresponding to the main symmetry points in the BZ. This information is relevant to modeling transport properties in ZnO and related nanostructures, using semiempirical methods.

While the description of phonon frequencies by empirical models is usually performed with a reasonable success, we recall that different calculations may yield similar frequency values but completely different phonon eigenvectors. The latter are responsible for the different selection rules and affect directly the measured intensities. Therefore a more stringent test for the calculations is obtained by comparing the calculated intensities with those observed experimentally, especially outside of the high-symmetry directions. These can be readily calculated using the following expressions:[40,41]

$$S(\mathbf{Q},\omega) = \sum_{\mathbf{G},\mathbf{q},j} \left| \sum_{\kappa} a_{\kappa}(\mathbf{Q},\mathbf{q},j) \right|^2 \delta(\mathbf{q}+\mathbf{G}-\mathbf{Q}) \times \delta[\omega(\mathbf{q},j)-\omega][1+n(\omega)]/\omega,$$

$$a_{\kappa}(\mathbf{Q},\mathbf{q},j) = b_{\kappa}\mathbf{Q}\cdot\mathbf{u}_{\kappa}(\mathbf{q},j)e^{-i\mathbf{Q}\cdot\mathbf{R}_{\kappa}}e^{-W_{\kappa}}, \quad (1)$$

where κ stands for zinc and oxygen, b_{κ} are the corresponding neutron-scattering lengths, $u_{\kappa}(\mathbf{q},j)$ and $\omega(\mathbf{q},j)$ the eigendisplacements, in Cartesian units, and phonon frequencies of j branch at $\mathbf{q}$ wave vector, respectively, and the exponential terms $e^{-W_{\kappa}}$ the Debye-Waller factors. Note that the mass dependence, one over the square root of the κ-atom mass, is hidden in the definition of the atomic eigendisplacements. The sum is performed over reciprocal lattice vectors $\mathbf{G}$, $\mathbf{Q}$ being the total momentum transfer, whereas the delta functions reflect the energy- and momentum-conservation laws.

Figure 2 displays the calculated intensity plots yielded by Eq. (1) for six representative scattering geometries corresponding to the phonon-dispersion relations along the Γ-K-M (110) (upper panels) and Γ-A (001) (lower panels) directions of the BZ. The visible branches have been labeled according to either their symmetry at the Γ point, or increasing in energy at the M point. In these calculations we neglected the contribution of the Debye-Waller factors. The plots were employed to define the strategy of the INS experiments. The selected scattering geometries (220, 009, and 008 Brillouin zones) in Fig. 2 exemplify the relevance of taking into account the eigenvectors and selection rules in order to maximize the throughput of IXS and INS experiments. The success in predicting the best conditions for the INS experiment to determine each phonon branch allowed the acquisition of a sizeable and valuable data set, as shown in Fig. 1. Knowledge of the eigenvectors becomes indispensable when analyzing special issues related to a specific branch, e.g., in superconductors or other phase-transition-related phonon-softening phenomena.

TABLE II. INS and calculated phonon frequencies of ZnO for selected high symmetry points in the Brillouin zone, in meV.

q point	INS	*Ab initio*
K		17.5
	18.2	18.0
	23.0	22.5
	29.2	29.2
	58.0	59.1
	60.9	60.7
	64.5	65.2
	67.0	66.3
M	12.1	10.6
	15.7	15.4
		16.4
	21.4	20.9
	29.2	29.2
	32.0	32.1
	53.2	55.2
	55.1	55.7
	58.6	60.3
	60.0	62.4
	67.4	67.3
	68.5	68.4
H	12.6	12.2
	21.1	20.5
	31.9	32.0
	55.5	56.2
	63.0	63.7
	67.2	66.8
L	13.8	13.7
	14.1	14.2
	32.7	33.2
	55.4	57.7
		57.9
	68.2	68.7
A	9.9	8.5
	22.5	23.4
	52.9	52.6
	69.7	69.0

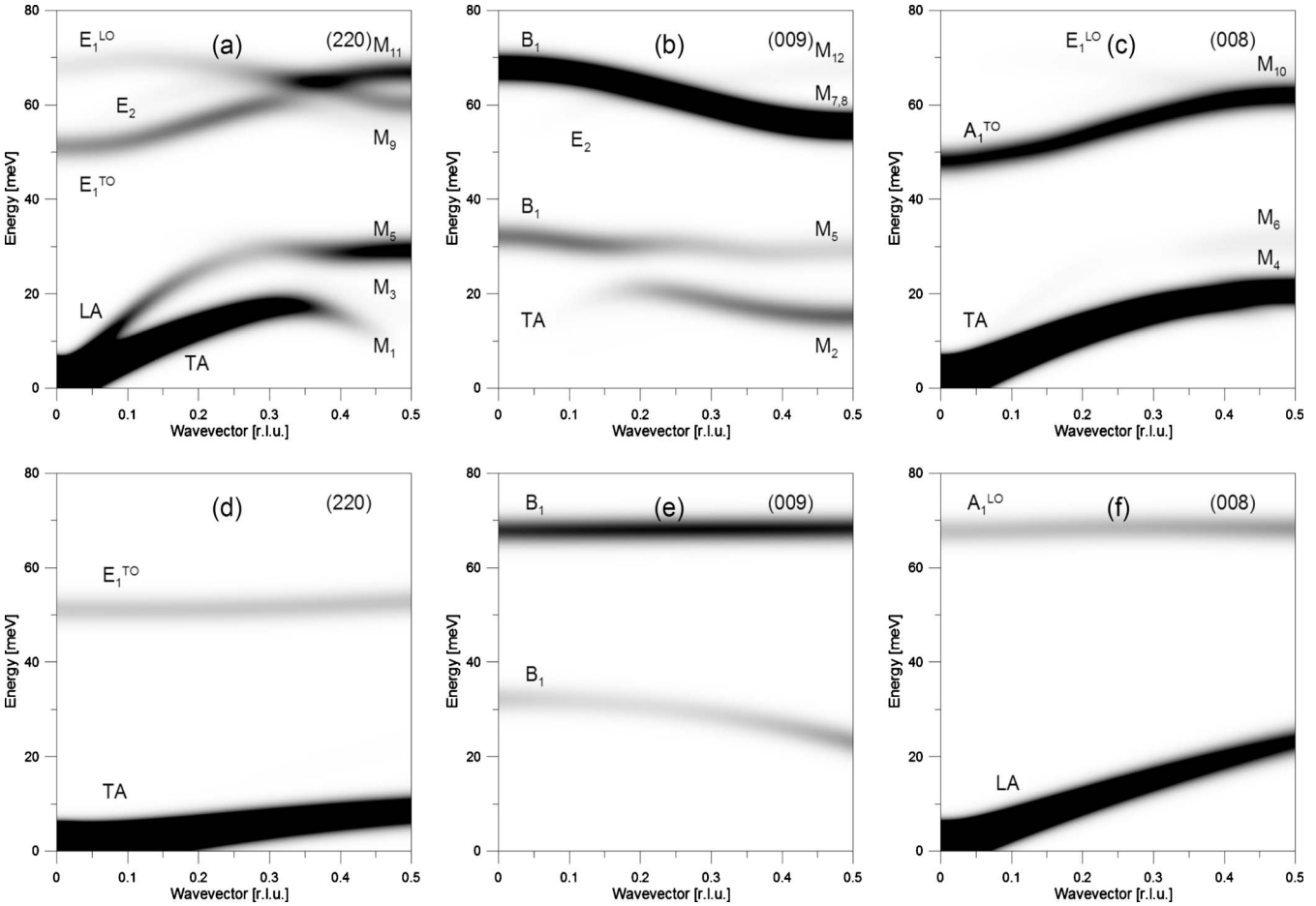

FIG. 2. Calculated scattering intensities in gray color scale for the phonon-dispersion relations along the Γ-*K*-*M* direction in the (a) 220, (b) 009, and (c) 008 Brillouin zones. Panels (d)–(f) display similar plots for the calculated intensities for phonons along the Γ-*A* direction. The *x*-axes show the phonon quasimomentum in r.l.u. from the Γ point to the border of the BZ whereas the *y*-axes display the phonon energy up to 80 meV. The intensities are calculated as indicated in the text, convolved with a Gaussian to take into account the finite resolution.

Considering that the wurtzite structure is relatively simple, several selection rules become apparent in these graphs, e.g., the silent mode B_1 is active in the BZ with an odd index for c^*, and therefore it appears in the 009 BZ but not in the 008 BZ, both along the Γ-*K*-*M* and along the Γ-*A* directions. Phonon band symmetry effects, such as the anticrossings at the *K* point in both acoustic and optical branches along the Γ-*K*-*M* direction and the anticrossing of B_1 branches at $q=0.2$ r.l.u. along the same direction are unveiled using this representation of the eigenvectors. The E_2 modes, on the contrary, are only excited if the scattering geometry has a reciprocal vector with a large component both in the a^*-b^* plane and along the c^* axis, such as the 224 BZ.

The wurtzite structure, as other hexagonal structures such as 4*H* and 6*H*, has a symmetry plane perpendicular to the *c* axis, which causes the folding of phonon branches along the c^*(Γ-A) direction. Half of them will be visible for an odd *k* index in the usual *hkl* notation for the BZ and the other half will appear only when selecting a scattering geometry involving an even *k* index. This fact is reflected in the alternation of longitudinal modes, either acoustic or optic, with B_1 modes. Likewise, transverse acoustic and optic modes alternate with E_2 modes.

As mentioned above, the A_1 and B_1 optical modes alternate due to symmetry along the Γ-A direction of the BZ. A more stringent test of the quality of *ab initio* eigenvectors consists of comparing calculated and scattering intensities for the two modes as a function of momentum transfer. Figure 3 displays the calculated and experimental intensities of the unfolded higher energy mode in the 008 BZ, normalized to the highest intensity, i.e., that of the B_1 mode at (0 0 9) r.l.u. The data from $\mathbf{q}=(0\ 0\ 8)$ to (0 0 8.5) correspond to the A_1 longitudinal optic mode, whereas those from (0 0 8.5) to (0 0 9) r.l.u. reflect the scattering strength of the upper B_1 mode, as expected from the selection rules. However, the *q* dependence of the calculated intensity deviates significantly from the experimental one, in particular, at (0 0 8) r.l.u. This may be correlated with the inaccurate description of the longitudinal optic modes at the Γ point. The calculated eigenvectors therefore provide a qualitative picture of the experimental intensities, though quantitative agreement is not fully achieved.

In conclusion, we have reported here INS measurements of the phonon-dispersion relations of bulk zinc oxide at low temperature. The experimental data are in excellent agreement with *ab initio* calculations for the phonon frequencies. Semiquantitative agreement is obtained for the scattered in-

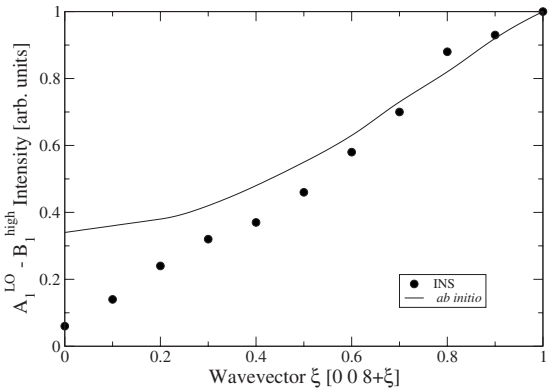

FIG. 3. Experimental and calculated intensity of high energy unfolded A_1-B_1 mode as a function of the momentum transfer from 008 to 009 BZs along the Γ-A direction, normalized to the maximum intensity. The x-axis is given in reciprocal lattice units.

tensities, thus validating the calculated phonon eigenvectors. The phonon frequencies obtained for the B_1 modes at the Γ point allow us to validate a previous assignment of disorder-activated induced modes observed in doped ZnO. The INS data presented here, together with those reported in the 1970s, yield a rather complete picture of the vibrational properties of ZnO, providing an experimental basis for semi-empirical models of interest in simulations of mechanical, thermodynamic, and transport properties of ZnO alloys, nanostructures and heterostructures.

ACKNOWLEDGMENTS

We are in debt to D. Crespo for a critical reading of the manuscript. We have benefited from fruitful discussions with J. Kulda and M. Jiménez-Ruiz. J.S. acknowledges financial support from the Spanish Ministry of Science and Innovation by CICYT under Grant Nos. MAT2007-60087 and ENE2008-04373, and by Generalitat de Catalunya under Grant No. 2009SGR1251. F.J.M. thanks the financial support from CICYT under Project No. CSD2007-00045, and the "Programa de Incentivo a la Investigación" of the Universidad Politécnica de Valencia under Project No. UPV2010-0096. A.H.R. has been supported by CONACyT Mexico under Project Nos. J-59853-F and J-83247-F. We acknowledge the computer resources provided by the CNS IPICYT, Mexico.

*jserrano@fa.upc.edu

[1] Y. C. Kong, D. P. Yu, B. Zhang, W. Fang, and S. Q. Feng, Appl. Phys. Lett. **78**, 407 (2001).
[2] X. D. Wang, C. J. Summers, and Z. L. Wang, Nano Lett. **4**, 423 (2004).
[3] A. Tsukazaki, M. Kubota, A. Ohtomo, T. Onuma, K. Ohtani, H. Ohno, S. F. Chichibu, and M. Kawasaki, Jpn. J. Appl. Phys., Part 2 **44**, L643 (2005).
[4] J. Goldberger, D. J. Sirbuly, M. Law, and P. Yang, J. Phys. Chem. B **109**, 9 (2005).
[5] M. H. Huang, S. Mao, H. Feick, H. Q. Yan, Y. Y. Wu, H. Kind, E. Weber, R. Russo, and P. D. Yang, Science **292**, 1897 (2001).
[6] K. Ramanathan *et al.*, Prog. Photovoltaics **11**, 225 (2003).
[7] M. Law, L. E. Greene, J. C. Johnson, R. Saykally, and P. D. Yang, Nat. Mater. **4**, 455 (2005).
[8] H. Kind, H. Q. Yan, B. Messer, M. Law, and P. D. Yang, Adv. Mater. **14**, 158 (2002).
[9] D. C. Look, Mater. Sci. Eng., B **80**, 383 (2001).
[10] S. J. Pearton, D. P. Norton, K. Ip, Y. W. Heo, and T. Steiner, J. Vac. Sci. Technol. B **22**, 932 (2004).
[11] U. Özgür, Ya. I. Alivov, C. Liu, A. Teke, M. A. Reshchikov, S. Doğan, V. Avrutin, S.-J. Cho, and H. Morkoç, J. Appl. Phys. **98**, 041301 (2005).
[12] S. J. Pearton, D. P. Norton, K. Ip, Y. W. Heo, and T. Steiner, Prog. Mater. Sci. **50**, 293 (2005).
[13] M. Krisch and F. Sette, Top. Appl. Phys. **108**, 317 (2007).
[14] T. Ruf, J. Serrano, M. Cardona, P. Pavone, M. Pabst, M. Krisch, M. D'Astuto, T. Suski, I. Grzegory, and M. Leszczynski, Phys. Rev. Lett. **86**, 906 (2001).
[15] M. Schwoerer-Böhning, A. T. Macrander, M. Pabst, and P. Pavone, Phys. Status Solidi B **215**, 177 (1999).
[16] W. Wegener and S. Hautecler, Phys. Lett. **31A**, 2 (1970).
[17] A. W. Hewat, Solid State Commun. **8**, 187 (1970).
[18] K. Thoma, B. Dorner, G. Duesing, and W. Wegener, Solid State Commun. **15**, 1111 (1974).
[19] T. C. Damen, S. P. S. Porto, and B. Tell, Phys. Rev. **142**, 570 (1966).
[20] S. P. S. Porto, B. Tell, and T. C. Damen, Phys. Rev. Lett. **16**, 450 (1966).
[21] J. M. Calleja and M. Cardona, Phys. Rev. B **16**, 3753 (1977).
[22] B. H. Bairamov, A. Heinrich, G. Irmer, V. V. Toporov, and E. Ziegler, Phys. Status Solidi B **119**, 227 (1983).
[23] J. Serrano, A. H. Romero, F. J. Manjon, R. Lauck, M. Cardona, and A. Rubio, Phys. Rev. B **69**, 094306 (2004).
[24] J. Serrano, F. Manjón, A. Romero, A. Ivanov, R. Lauck, M. Cardona, and M. Krisch, Phys. Status Solidi B **244**, 1478 (2007).
[25] The ABINIT code is a common project of the Université Catholique de Louvain, Corning Incorporated, and other contributors (http://www.abinit.org).
[26] X. Gonze, Phys. Rev. B **55**, 10337 (1997).
[27] X. Gonze and C. Lee, Phys. Rev. B **55**, 10355 (1997).
[28] X. Gonze *et al.*, Comput. Mater. Sci. **25**, 478 (2002).
[29] J. Serrano, F. Widulle, A. H. Romero, A. Rubio, R. Lauck, and M. Cardona, Phys. Status Solidi B **235**, 260 (2003).
[30] J. Serrano, F. J. Manjón, A. H. Romero, F. Widulle, R. Lauck, and M. Cardona, Phys. Rev. Lett. **90**, 055510 (2003).
[31] J. Serrano, R. K. Kremer, M. Cardona, G. Siegle, A. H. Romero, and R. Lauck, Phys. Rev. B **73**, 094303 (2006).
[32] N. Troullier and J. L. Martins, Phys. Rev. B **43**, 1993 (1991).
[33] J. P. Perdew and Y. Wang, Phys. Rev. B **45**, 13244 (1992).
[34] J. P. Perdew, K. Burke, and M. Ernzerhof, Phys. Rev. Lett. **77**, 3865 (1996).
[35] L. Hedin, Phys. Rev. **139**, A796 (1965).

[36] M. Oshikiri and F. Aryasetiawan, Phys. Rev. B **60**, 10754 (1999).
[37] M. Oshikiri and F. Aryasetiawan, J. Phys. Soc. Jpn. **69**, 2113 (2000).
[38] F. Reuss, C. Kirchner, T. Gruber, R. Kling, S. Maschek, W. Limmer, A. Waag, and P. Ziemann, J. Appl. Phys. **95**, 3385 (2004).
[39] F. J. Manjón, B. Marí, J. Serrano, and A. H. Romero, J. Appl. Phys. **97**, 053516 (2005).
[40] D. Strauch, B. Dorner, A. Ivanov, M. Krisch, A. Bosak, J. Serrano, W. Choyke, B. Stojetz, and M. Malorny, Mater. Sci. Forum **527-529**, 689 (2006).
[41] A. Bosak, K. Schmalzl, M. Krisch, W. van Beek, and V. Kolobanov, Phys. Rev. B **77**, 224303 (2008).